Nanoscale

Elucidating the assembly of Nanoparticle Organic Hybrid Materials (NOHMs) near an electrode interface with varying potential using Neutron Reflectivity

Journal:	*Nanoscale*
Manuscript ID	NR-ART-12-2023-006621.R1
Article Type:	Paper
Date Submitted by the Author:	21-Mar-2024
Complete List of Authors:	Haque, Md Ashraful; The University of Tennessee Knoxville, Chemistry Hamilton, Sara ; Columbia University Feric, Tony; Columbia University Park, Ah-Hyung; Columbia University, Department of Earth and Environmental Engineering & Department of Chemical Engineering Dadmun, Mark; The University of Tennessee Knoxville, Chemistry

Elucidating the assembly of Nanoparticle Organic Hybrid Materials (NOHMs) near an electrode interface with varying potential using Neutron Reflectivity

Md Ashraful Haque[a], Sara T. Hamilton[c,d] ,Tony G. Feric[b,d], Ah-Hyung Alissa Park[b,c,d],

Mark D. Dadmun[a*]

[a]Department of Chemistry

The University of Tennessee, Knoxville, TN, 37996, USA

[b]Department of Chemical Engineering,

Columbia University, New York, NY 10027, USA

[c]Department of Earth and Environmental Engineering,

Columbia University, New York, NY 10027, USA

[d]Lenfest Center for Sustainable Energy, The Earth Institute, Columbia University

Abstract

A critical concern regarding electrolyte formulation in an electrochemical environment is the impact of the interaction of the multiple components (i.e., supporting electrolyte or additive) with the electrode surface. Recently, liquid-like neat Nanoparticle Organic Hybrid Materials (NOHMs) have been considered as an electrolyte component to improve the transport of redox-active species to the electrode surface. However, the structure and assembly of the NOHMs near the electrode surface is unknown and could significantly impact the electrode-electrolyte interface. Hence, we have investigated the depth profile of polyetheramine (HPE) polymer and NOHM-I-HPE (nanoparticles with ionically bonded HPE polymer) in deuterated water (D_2O) in the presence of two different salts ($KHCO_3$ and $ZnCl_2$) near two different electrode surfaces using neutron reflectometry. Moreover, the depth profile of the NOHM-I-HPE near the electrode surface in a potential has also been studied with in-situ reflectivity experiments. Our results indicate that a change in the chemical structure/hydrophilicity of the electrode surface does not significantly impact the ordering of HPE polymer or NOHM-I-HPE near the surface. This study also indicates that the NOHM-I-HPE particles form a clear layer near the electrode surface immediately above an adsorbed layer of free polymer on the electrode surface. The addition of salt does not impact the layering of NOHM-I-HPE, though it does alter the conformation of the polymer grafted to the nanoparticle surface and free polymer sequestered near the surface. Finally, the application of negative potential results in an increased amount of free polymer near the electrode surface. Correlating the depth profile of free polymer and NOHM-I-HPE particles with the electrochemical performance indicates that this assembly of free polymer near the electrode surface in NOHM-I-HPE solutions contributes to the higher current density of the system. Therefore, this holistic study

offers insight into the importance of the assembly of NOHM-I-HPE electrolyte and free polymer near the electrode surface in an electrochemical milieu on its performance.

Introduction

The use of Redox Flow Battery (RFB) has been considered as a potential solution to tackle a common renewable energy storage relevant issue, that is the incorporation of this source into grid-scale energy storage infrastructure.[1,2] RFBs possess significant advantages over common lithium-ion batteries, specifically, the ability to separate cathodic and anodic electrolyte, which allows RFB to scale up power delivery and energy density without requiring any effort to change the design for specific applications.[3–6] However, the electrolytes used in RFBs still suffer from limited solubility of electro-active species, safety concerns and expensive raw materials.[7,8] Recently, deep eutectic solvents,[9–11] microemulsions[12–15] and Nanoparticle Organic Hybrid Materials (NOHMs)[16–19] have been considered as novel electrolytes for RFBs. Among these novel electrolytes, NOHMs are of particular interest as they have shown great potential to be used in RFBs due to their low volatility,[20] increased oxidative thermal stability[19,21–24] and chemical tunability.[25,26]

Recently, significant research efforts have been undertaken to understand the structure and assembly of NOHMs and correlate this to their transport behavior to provide insight to optimally deploy them in electrochemical applications.[17,18,27–29] Specifically, in our previous study, small-angle neutron scattering (SANS) is used to elucidate the structure and assembly of ionic NOHMs, which highlights that in an aqueous solution, large amount of polymer that is ionically grafted to the nanoparticle can detach from the grafting site and thus alters the composition of the solvent. Moreover, this *free polymer* can interact with the grafted polymer while altering the conformation

of the grafted polymer. Our study also indicates that the addition of salt changes this assembly of polymer as salt competes with the polymer for the grafting site on the nanoparticle. The presence of free polymer and alteration of the polymer conformation and NOHMs assembly with the addition of salt significantly impacts the transport behavior of supporting electrolytes via NOHMs in the bulk and near the electrode.[30]

Literature shows that a very common cause of unstable current output is the result of dendrite formation from the uneven deposition of salt.[31–33] The presence of polymeric additives has been shown to improve the process of smooth deposition of salt on the electrode surface.[29,34] A recent study by Hamilton et al. investigated the near surface ordering of ionic NOHMs (NOHM-I-HPE) with HPE polymer in the presence of $ZnCl_2$ salt through various spectroscopic and electrochemical analyses. The study indicates that the presence of HPE polymer and NOHM-I-HPE at a certain composition in relation to Zn salt can maintain a stable current output and assists in the smooth deposition of Zn . However, a thorough investigation is still required to understand the packing of NOHM-I-HPE near the electrode surface and its impact on Zn salt deposition. Hence, this study uses Neutron Reflectometry (NR) to investigate the ordering of NOHM-I-HPE and HPE polymer near electrode surface, including the impact of an added potential on this near surface structure.

Neutron Reflectometry is a unique technique that allows the investigation of the depth profile of structures having different composition and densities.[35] Moreover, isotope-specific interaction of neutrons eases the process of discerning protonated species, such as polymers, from deuterated species, such as the deuterated solvent.[36] NR has been used extensively to investigate the ordering of different ionic liquid-based electrolytes near electrode interfaces.[37–40] The technique is also used to highlight the ordering of nanoparticles near modified surfaces.[41,42] In this

study, we investigate the ordering of HPE polymer and NOHM-I-HPE, considered as electrolyte additives, near two different electrode surfaces (SiO_x and Au). Previous studies indicated that surface hydrophilicity altered the ordering of soft materials near a surface.[43] Thus, examining the ordering of the NOHMs near two different surfaces provides insight into the importance of surface hydrophilicity on NOHMs ordering, where the modified SiO_x interface (water contact angle ~40°), is more hydrophilic than Au (water contact angle ~ 70°). Moreover, we have investigated the near surface ordering of the additives in the presence of supporting electrolyte, 0.1M $KHCO_3$, near both interfaces. Finally, we have examined the ordering of NOHM-I-HPE near the Au electrode in the presence of 0.1M $ZnCl_2$ salt with and without applied potential. Under constant current conditions, the observed applied potential allowed us to provide insight into the impact of the NOHM-I-HPE, and its near surface assembly, on the process of Zn deposition occurring at the electrode surface.

Experimental Section

NOHM-I-HPE Preparation

NOHM-I-HPE was synthesized using previously reported methods.[16,17,19,25,29] Briefly, 6 wt. % 3-(trihydroxysilyl)-1-propane sulfonic acid (Gelest, Inc.) and 3 wt.% silica nanoparticles (Ludox HS-30, 7 nm, Sigma Aldrich) aqueous solutions were prepared, followed by the addition of the silica suspension to the silane solution in a dropwise manner. This was followed by the addition of 1 M NaOH to adjust the solution pH to 5. The resulting solution was stirred for 24 h at 70 °C, facilitating the grafting reaction between the silica nanoparticle and the linker. Excess linker present was removed via dialysis (SnakeSkin Dialysis Tubing 3500 molecular weight cut-off (MWCO), Thermo Scientific) against deionized water for 48 hours. The linker-grafted solution was passed through a cation exchange resin column (Dowex HCR-W2, Sigma-Aldrich) for

removal of any cations on the functionalized SiO_2 nanoparticles surface and protonation of the linker sulfonate groups. In order to ionically tether the polymer canopy to the surface-modified nanoparticles, a solution of 10 wt.% Jeffamine M2070 (HPE, MW 2000, Huntsman Co.) was prepared and added dropwise to the functionalized nanoparticle suspension until the equivalence point of the solution was reached (pH = 6.5), where all the linker sulfonate groups were neutralized. Finally, the solution was oven dried overnight at 65 °C to remove all water from the prepared mixture. Before sample preparation, NOHM-I-HPE materials were dried again under vacuum at 60 °C for 3 h to ensure the removal of any possible absorbed moisture.

NOHM-I-HPE and HPE Solution Preparation

NOHM-I-HPE and HPE solutions were prepared by mixing previously oven dried NOHM-I-HPE and HPE with D_2O to achieve 10 wt.% in solution using an analytical balance (ML104T, Mettler Toledo) with a precision of 10^{-4} g. For samples containing salt, the solutions were prepared by adding 0.1 M $KHCO_3$ (Sigma-Aldrich, ACS, ≥99.0%) or 0.1 M $ZnCl_2$ (Sigma Aldrich, ACS, ≥99.0%) to the previously prepared NOHM-I-HPE and HPE solutions. Samples were mixed in 10 mL volumetric flasks until complete dissolution of the salt was observed. The pH of the solutions containing $ZnCl_2$ was adjusted to 5.0 using H_3BO_3 (Sigma Aldrich, ACS, ≥99.0%).

Surface Preparations

Au and SiO_x surfaces were prepared in advance of the execution of the neutron scattering experiments. The Au wafer which has a chromium layer for better adhesion of the gold layer, was provided by Oak Ridge National Laboratory's Center for Nanophase Materials Science (CNMS). For the preparation of SiO_x surface, the silicon wafer was first cleaned with a piranha solution prepared using 3:1 sulfuric acid:hydrogen peroxide to remove contaminants from the surface. Then

the wafer was rinsed using nanopure water and dried using air. The wafer was then sealed in air for several days to form oxide layer.

Neutron Reflectivity Measurement and Analysis

Neutron reflectivity experiments were conducted at the BL-4B liquid reflectometer at the Oak Ridge National Lab (ORNL), Spallation Neutron Source (SNS). A solution cell was used to load the samples and then measurements were obtained at 25 °C over a Q range of 0.008-0.2 $Å^{-1}$. The solution cell used for these measurements is detailed by Browning et al.[44] In brief, the cell consists of an aluminum housing in which the experimental wafer (Au or SiOx) and a 2″ Si wafer are separated by an O-ring. Once the cell is compressed against the O-ring, a space is created that can be filled with ~ 3 ml of the solution. The solution was injected carefully through the liquid inlets created on the Si wafer so that no air bubbles were present. During the sample changeover, the cell was flushed with the sample that is planned for the next experiment to remove any residue from the earlier experiments. Before the cell assembly, the parts of the cell were sonicated in hexane and isopropanol for cleaning purposes.

To execute the potential-dependent experiments, a 3-electrode electrochemical cell was prepared that was comprised of a counter electrode (platinum), a working electrode (Au) and a reference electrode (Ag/AgCl). Potential dependent analysis at -1.1 V and -1.5 V (vs Ag/AgCl) was performed using a Biologic VSP potentiostat. When the desired potential was reached, the cell was held for two hours to obtain neutron reflectivity measurements. Before switching the potential from -1.1 V to -1.5 V, the cell potential was turned off and held at rest for 10 minutes. Figure S1 shows the photo of the electrochemical cell used for the neutron reflectivity measurements.

All reflectivity data was reduced by the instrument scientist and fit using the Motofit package loaded as an extension in the IGOR Pro software.[45] Neutron reflectivity is a sensitive technique that provides information on the depth profile of a layered structure. The reflectivity fit provides information about the thickness, roughness and scattering length density of the layered structures. The scattering length density (SLD) documents the identity of the specific species probed within the density profile. The SLD of a given species can be calculated using Equation 1.

$$SLD\ (z) = \sum b_i\, n_i(z) \qquad \mathbf{1}$$

In Equation 1, SLD ($Å^{-2}$) is the scattering length density of the species, b_i is the scattering length (fm) of individual nuclei, n_i is the number density of the species and z is the perpendicular distance away from the substrate surface. The calculated scattering length densities of the known components in the systems studied are provided in Table S1.

Discussion and Results

Characterization of SiO_x and Au substrates

The density profile of the Au and SiO_x wafers is first characterized by neutron reflectometry. Figure S2 shows the reflectivity curves and the fit of these curves to a scattering length density profile for both wafers. The substrates have known composition with unspecified density profiles, which are characterized by thickness (Z) and roughness (R) of layers. Therefore, while fitting the reflectivity profile of the substrates, the SLD of each was not allowed to vary. The results from the reflectivity fitting confirm the formation of an SiO_x layer with an SLD of 2.89 $x10^{-6}$ $Å^{-2}$ with a thickness of ~135 Å thick. Two Au-coated wafers are used for reflectivity analysis to minimize the sample change time. The reflectivity analysis of the Au coated Si wafers show a 46-56 Å thick chromium layer with a subsequent Au coated layer of 140 Å. Table S2 documents

the SLD, thickness and roughness of density profile of the SiO_x and Au coated wafers. The SLD, thickness and roughness of the density profile on these substrates were kept constant in the fitting and analyses of wafers in contact with HPE or NOHMs solutions to increase the confidence of the fit. However, while fitting the NR profiles of HPE sample with the SiOx substrate, it was realized that the SiO_x surface hydrates in the presence of deuterated water, increasing the SLD from 2.89 $x10^{-6}$ $Å^{-2}$ to 3.49 $x10^{-6}$ $Å^{-2}$. The increase in SLD with the presence of deuterated water molecules of SiO_x surface is previously observed when a microemulsion sample is analyzed for structural variation with a change in hydrophilicity of the surface.[46] The obtained SLD (3.49 $x10^{-6}$ $Å^{-2}$) of the SiO_x surface was then kept constant to obtain a robust fit for the density profile of the HPE polymer with salt and NOHM-I-HPE sample with and without salt.

Density Profile of HPE polymer near Au and SiO_x substrate

To simplify the analysis of the ordering of NOHMs near the Au and SiO_x interfaces, we first investigate the near surface structure of 10 wt.% HPE polymer with and without salt using neutron reflectometry. Figure 1 shows the reflectivity curve and fit of the density profile of HPE polymer in D_2O near the Au surface, where the inset in Figure 1 shows the SLD profile obtained from the fit. Table 2 documents the details of the density profile obtained from reflectivity fit.

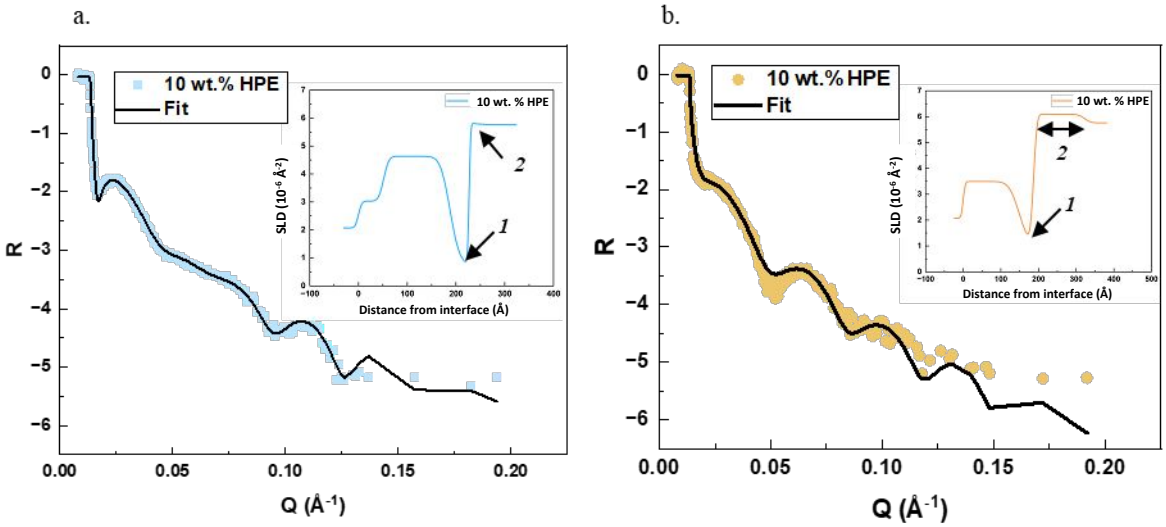

Figure 1. Neutron reflectivity profiles of HPE polymer in D2O near Au surface (a) and SiO_x surface (b). The inset contains the SLD profile obtained from the fit, where the two layers are noted in the SLD profile: *1* is the polymer rich layer and *2* is water rich layer.

The reflectivity results indicate that layers with an SLD of 0.78 and 1.00 (the unit of SLD x10^{-6} $Å^{-2}$ is omitted for simplification) decorate near the Au and SiO_x surfaces, respectively. The SLD of this layer is similar to the SLD of the pure HPE polymer documented in Table S1. Hence, we interpret this to indicate that an HPE-rich layer forms near both surfaces. Moreover, the thickness of the HPE-rich layer near both surfaces is ~38 Å. Small-angle neutron scattering shows that the radius of gyration (R_g) of the HPE polymer is ~15 Å,[19] indicating that two-three layers of HPE polymer assemble near the interfaces. The roughness of the HPE-rich layer is on the length scales of ~16-20 Å, where such a high roughness indicates a broad interface between the HPE rich layer to the subsequent layer. The SLD of this subsequent layer 5.85 on Au and 6.09 on SiO_x , which is approaching the SLD of pure D_2O (6.35). Hence, this layer is a D_2O-rich layer. The thickness of the D_2O-rich layer near Au surface is only 16 Å whereas the D_2O-rich layer near the SiO_x is 135 Å. The hydrophilic nature of SiO_x could contribute to the broader D_2O layer near the surface.

Impact of $KHCO_3$ salt in the ordering of HPE polymer

Figure 2 shows SLD profile that emerges from the fit of the reflectivity profile of HPE polymer with added $KHCO_3$ salt neighboring both the Au and SiO_x surfaces. Table 2 documents the details of the SLD density profile that emerge from the fit of the reflectivity data. The SLD of the first layer is ~0.60, where such a low value confirms the presence of an HPE-rich layer near both surfaces. The thickness of the HPE polymer layer is ~37 Å on both surfaces, with roughnesses close to 10 Å confirming a multilayer of the HPE polymer. Unlike the sample with no salt solution, the density profile of the subsequent layers near both interfaces reveals three unique HPE-rich layers in both the Au and SiO_x samples. However, the variation of the SLDs and thicknesses in the

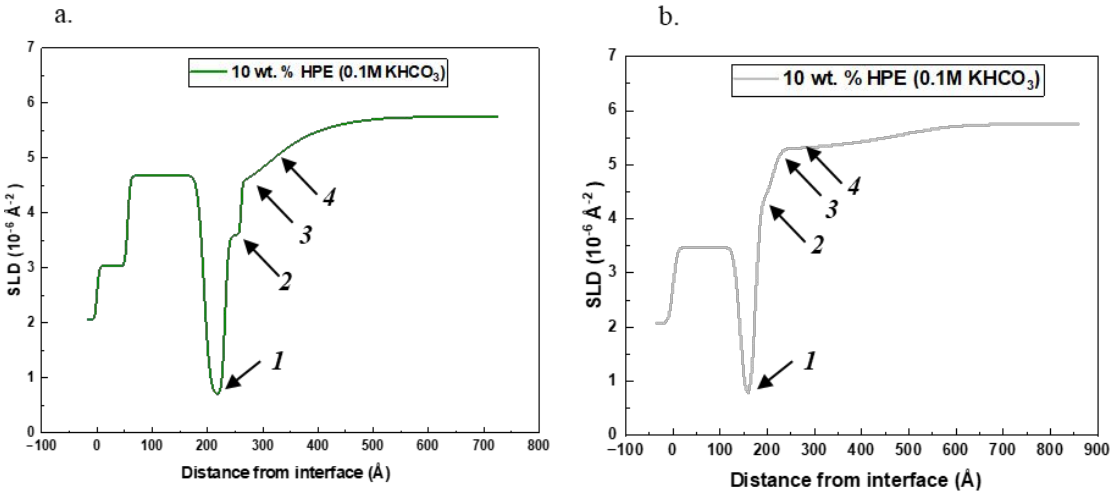

Figure 2. SLD profiles of HPE polymer in D_2O with the presence $KHCO_3$ salt near Au surface (a) and SiO_x surface (b). 4 layers are documented in the SLD profile: *1* is the polymer rich layer and *2, 3, 4* are the water rich layer .

density profiles are quite different depending on the interfaces.

In the case of the Au surface, the density profile approximates three layers neighboring the HPE polymer-rich layer, where the SLDs of the three layers are 3.46, 4.37, and 5.12. The SLD of 3.46 is well above that of the pure HPE polymer, indicating that this layer is more D_2O rich than the near surface layer, where the amount of D_2O increases with each subsequent layer. However, the SLD of these layers near the SiO_x surface is higher than that observed near the Au surface.

This indicates that D_2O aggregates more in the vicinity of the (hydrophilic) SiO_x surface. In fact, the average thickness of the three D_2O rich layers near the SiO_x surface is larger than the same three D_2O rich layers near the Au surface, further documenting the affinity of D_2O to the SiO_x surface.

Table 2. SLD profile obtained from fitting of the reflectivity profiles of 10 wt.% HPE polymer and 10 wt.% HPE polymer with 0.1M $KHCO_3$ in D_2O near Au and SiO_x surfaces.

Sample	Wafers	Parameters	Layer 1	Layer 2	Layer 3	Layer 4	Bulk
10 wt.% HPE	Au	SLD (10^{-6} Å^{-2}) ± error	0.78 ± 0.15	5.85 ± 0.02			5.76
		Z (Å) ± error	36.8 ± 1.63	16.1 ± 2.76			-
		R (Å) ± error	15.9 ± 0.20	2.69 ± 1.90			17.1 ± 5.98
	SiO_x	SLD (10^{-6} Å^{-2}) ± error	1.00 ± 0.04	6.09 ± 0.03			5.76
		Z (Å) ± error	37.8 ± 0.94	135 ± 2.16			-
		R (Å) ± error	21.7 ± 0.92	7.25 ± 0.33			13.3 ± 1.15
10 wt.% HPE 0.1M $KHCO_3$	Au	SLD (10^{-6} Å^{-2}) ± error	0.65 ± 0.03	3.46 ± 0.24	4.37 ± 0.07	5.12 ± 0.08	5.75
		Z (Å) ± error	38.4 ± 0.47	29.1 ± 2.40	45.2 ± 17.3	69.1± 4.58	-
		R (Å) ± error	8.91 ± 1.48	4.73 ± 2.62	11.03 ± 7.22	49.5 ± 12.9	86.1± 49.16
	SiO_x	SLD (10^{-6} Å^{-2}) ± error	0.67 ± 0.15	4.33 ± 0.13	5.28 ± 0.05	5.36 ± 0.01	5.75
		Z (Å) ± error	35.8 ± 2.16	46.1 ± 1.41	97.5 ± 11.5	197 ± 7.40	-
		R (Å) ± error	13.4 ± 0.94	7.47 ± 1.14	5.14 ± 2.46	51.3 ± 11.3	90.9 ± 8.76

This phenomenon of ordering water molecules in different layers near both substrates can be attributed to the kosmotropic effect of the salt.[47,48] The salt is dissociated to ions in the water ,

where the electron density of the ions guides the dipolar water molecules to reorient around the ionic species, which results in a structure of water molecules that differs from that of bulk water. Kosmotropic salts promotes the ordering of water, whereas chaotropic salts disrupt the water structure.[49] The kosmotropic behavior of the $KHCO_3$ salt can mediate the ordering of the water by altering arrangement of water molecules around K^+ and HCO_3^- ions.[50] However, it is not clear from the SLD profiles whether the K^+ or HCO_3^- ionic species dominates the water ordering in these layers.

Density profile of NOHM-I-HPE near Au and SiO_x surface

The near surface assembly of NOHM-I-HPE near the Au and SiO_x surface is determined by fitting the reflectivity profile of the 10 wt.% NOHM-I-HPE solutions near the SiO_x and Au surfaces. Figure 3 shows the SLD profile of NOHM-I-HPE near the Au and SiO_x surface resulted

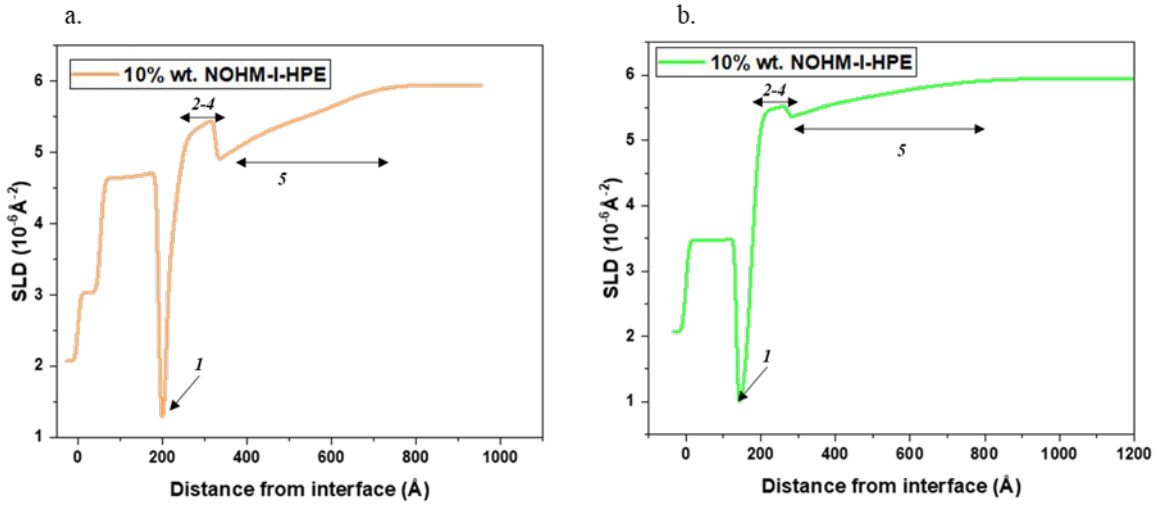

Figure 3. SLD profiles of NOHM-I-HPE in D_2O near Au surface (left) and SiO_x surface (right). 5 layers are noted in the figure: layer *1* is the free polymer layer, layer *2-4* forms the single NOHMs layer and layer *5* is the transition layer.

from the fit of the reflectivity curves. Table 3 documents the details of the SLD density profile that emerge from the fit of the reflectivity data of NOHM-I-HPE solution near both interfaces.

Table 3 Density profile parameters that result from fitting the reflectivity profile of 10 wt.% NOHM-I-HPE and 10 wt.% NOHM-I-HPE with 0.1M $KHCO_3$ in D_2O.

Sample	Wafer	Parameters	Layer 1	Layer 2	Layer 3	Layer 4	Layer 5	Bulk
10 wt.% NOHM-I-HPE	Au	SLD (10^{-6} Å^{-2}) ± error	0.80 ± 0.15	2.70 ± 0.03	5.01 ± 0.05	4.38 ± 0.08	5.51 ± 0.01	5.95
		Z (Å) ± error	18.7 ± 0.71	18.3 ± 0.56	97.7 ± 0.34	21.9 ± 1.67	285± 22.0	-
		R (Å) ± error	3.54 ± 0.81	5.69 ± 0.27	18.6 ± 2.82	4.95 ± 0.88	117 ± 2.62	80.5± 11.47
	SiO_x	SLD (10^{-6} Å^{-2}) ± error	0.83 ± 0.15	1.21 ± 0.41	5.39 ± 0.01	5.18± 0.11	5.47 ± 0.19	5.95
		Z (Å) ± error	26.6 ± 3.29	19.8± 1.86	105.83 ± 7.10	20.8 ± 0.80	242± 2.62	-
		R (Å) ± error	4.73 ± 0.01	6.89 ± 3.05	16.4 ± 1.20	6.05 ± 2.10	81.5 ± 8.52	188± 10.1
10 wt.% NOHM-I-HPE 0.1M $KHCO_3$	Au	SLD (10^{-6} Å^{-2}) ± error	1.18 ± 0.08	2.94 ± 0.28	4.54 ± 0.01	4.04 ± 0.08	5.35± 0.44	5.9
		Z (Å) ± error	14.9 ± 0.23	14.4 ± 0.42	91.7 ± 1.41	14.6 ± 0.21	221 ± 4.96	
		R (Å) ± error	5.92 ± 1.1	4.77 ± 1.0	21.9 ± 3.80	6.48 ± 0.80	24.41 ± 8.04	60.2± 21.2
	SiO_x	SLD (10^{-6} Å^{-2}) ± error	0.71 ± 0.01	1.03 ± 0.01	5.21± 0.01	4.99 ± 0.01	5.70 ± 0.08	5.9
		Z (Å) ± error	19.8 ± 0.1	17.8 ± 0.04	85.6± 1.5	10.0 ± 1.8	303 ± 9.10	-
		R (Å) ± error	5.40 ± 1.10	8.29 ± 1.27	16.5 ± 0.73	6.95 ± 1.70	30.36 ± 5.71	76.1± 26.84

The results from the reflectivity fit of the NOHM-I-HPE solution show a structure of 5 layers above the Au and SiO_x surfaces and below the bulk NOHM-I-HPE solution. The first layer has a low SLD of ~0.84 near both the Au and SiO_x surface, which is very similar to the SLD obtained from reflectivity profiles of HPE polymer in D_2O. The thickness of the layer varies from ~15-27 Å, similar to the R_g of the polymer. The second, third, and fourth layers oscillate between a narrow layer (~20 Å) with an SLD of 2.70 (Au surface) and 1.21 (SiO_x surface), followed by a layer with a much larger SLD (5.01 on Au and 5.39 on SiO_x) that is ~100 Å wide, with the fourth

layer that is also narrow (~20 Å) with a lower SLD (4.38 on Au and 5.18 on SiO_x). Given the thicknesses of these layers, and their SLDs, we interpret this SLD profile to indicate the ordering of a single fluctuating layer of NOHMS in D_2O immediately above the HPE rich layer. In this picture, the first layer captures the lower part of the NOHMs layer, which is the grafted HPE on the bottom of the silica nanoparticle; the second layer is the silica nanoparticle dispersed in D_2O, and the fourth layer is the HPE grafted on the top of the nanoparticle. The thickness and SLD of the third layer is consistent with the silica nanoparticle diameter (~90 Å)[30] and scattering length density. The SLD of this layer is higher than the SLD of the pure silica nanoparticle (5.0-5.4 vs 4.2), which makes sense, as this layer must also include D_2O. The roughness (~17 Å) of this layer is consistent with the fluctuating nature of this NOHMs layer in the z-direction. The fifth layer is a transition layer to the bulk layer that has an SLD of 5.51 and 5.47 near the Au and SiO_x interfaces, respectively. This is the highest SLD among the five layers, which signifies the significant contribution of higher D_2O content in this layer than lower layers.

Overall, the ordering profile of the NOHM-I-HPE near the Au and SiO_x surface shows an interesting assembly, where Figure 4 provides an illustration of the ordering of the NOHMs and HPE near the surface in the NOHM-I-HPE solution from the reflectivity analysis. This cartoon

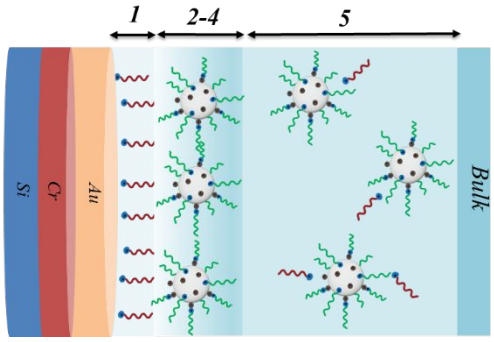

Figure 4 Representative figure illustrating the ordering of free polymer and NOHM-I-HPE near Au surface. 5 layers are noted in the figure: layer *1* is the free polymer layer, layer *2-4* forms the single NOHMs layer and layer *5* is the transition layer.

captures the presence of a single HPE-rich layer near both interfaces. This single layer of HPE polymer can be attributed to the *free polymer* that is present in NOHM-I-HPE solution. Then an ordered NOHMs layer is observed above the free polymer layer, a combination that is captured in the second, third and fourth layers from the reflectivity fit. This is capped by a transition layer that extends to the bulk of the solution. Moreover, we believe that the assembly of the NOHMs into this stratification emerges from the affinity of the HPE layer to the surface, where the subsequent organization of the NOHMs above this layer is guided by this foundational layer.

Impact of $KHCO_3$ salt on the ordering of NOHM-I-HPE near Au and SiO_x surface

The addition of $KHCO_3$ salt to the NOHM-I-HPE does not alter the overall assembly structure of the NOHM-I-HPE near the surface. Analysis of the reflectivity profiles shows that the density profile of the NOHMS in the presence of the $KHCO_3$ salt forms five layers that mimic the structure in the unsalted NOHMs solutions. Figure 5 shows the SLD profiles of the NOHM-I-HPE solutions with added $KHCO_3$ salt and Table 3 documents the details of the SLD depth profile near both surfaces.

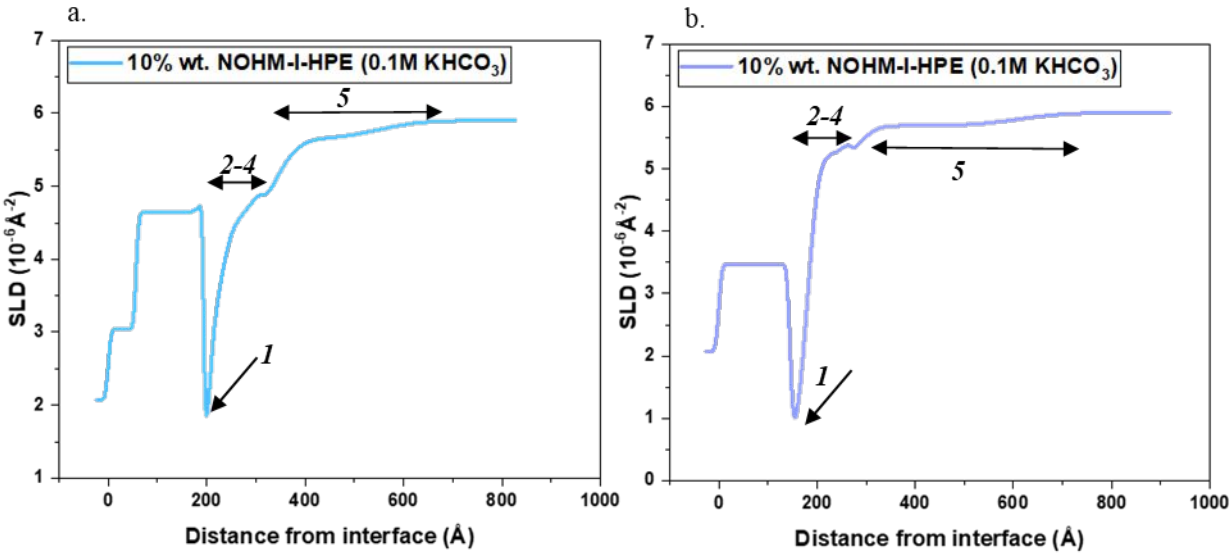

Figure 5 SLD profiles of NOHM-I-HPE in D_2O in the presence of $KHCO_3$ salt near Au surface (a) and SiO_x surface (b). 5 layers are noted in the figure: layer *1* is the free polymer layer, layer *2-4* forms the single NOHMs layer and layer *5* is the transition layer.

Although the density profile of the NOHMs with solution added salt exhibit similar ordering to those without salt, careful analysis shows notable changes that can be attributed to the role of salt on the nanoscale structure in the solution. For instance, the size of the HPE-rich layer near the surface decreases for both surfaces, while the thickness of the grafted HPE polymer layers decreases from ~19 Å to ~14 Å and ~22 Å to ~15 Å. Thus, the presence of the salt tends to decrease the solvent quality and collapses the HPE polymer in solution. This is consistent with our small-angle neutron scattering results, which quantifies the impact of adding salt on the conformation of the free and grafted HPE polymer.[19,30]

Density profile of NOHM-I-HPE near Au surface with varying potential:

The results presented above provide insight into the density profile of NOHM-I-HPE solutions near a quiescent surface. However, it is clear that the application of a potential across this interface can alter the structure of the interface, i.e., by deposition of salt, and it is known that a field can alter the orientation and structure of soft materials. Thus, we completed experiments to monitor the near surface density profile of the NOHMs solutions with $ZnCl_2$ salt in an applied field. In these experiments, the sample was under the influence of applied potential at 0, -1.1, -1.5 V vs Ag||AgCl. Comparing the reflectivity profile of the NOHM-I-HPE solutions with $ZnCl_2$ with 0 V and -1.1 V applied field are presented in Figure 6. Inspection of this figure clearly shows a shift in the fringes with application of -1.1 V, indicative

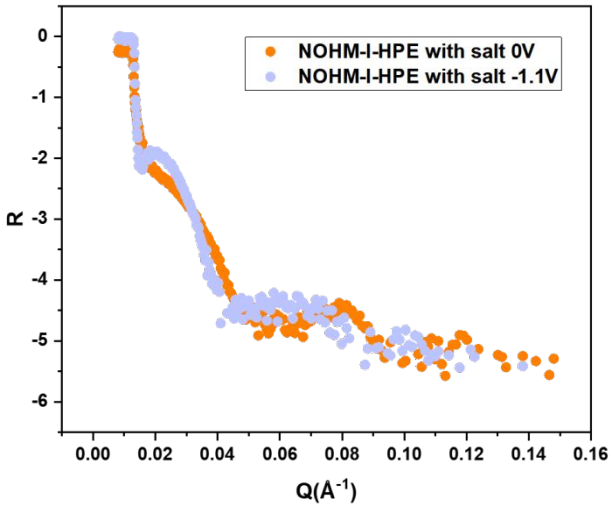

Figure 6 Neutron reflectivity profile showing change in features in reflectivity profile when potential is applied to NOHM-I-HPE solution in presence of $ZnCl_2$ salt.

of a change in the density profile of the near surface structure of the NOHMs solutions with the applied potential. Figure 7 shows the SLD profiles of NOHM-I-HPE solutions with added $ZnCl_2$ at 0 V, -1.1 V, and -1.5 V, from the fits of the data. Table 4 provides the details of the density profile of the SLD that emerge from the fit.

The ordering of NOHM-I-HPE with the presence of $ZnCl_2$ salt without any potential shows a similar structure to those observed in NOHM-I-HPE solutions with $KHCO_3$ salt. The profile shows the presence of 5 layers between the Au surface and bulk solution. The SLD of the layer neighboring the Au surface is 2.88, while its thickness is ~15 Å. It is interesting that this layer has a higher SLD than that of the NOHM-I-HPE solution with $KHCO_3$ salt, indicating that this layer contains more than just HPE polymer. An increased amount of D_2O in this layer or the coordination of the Zn ion with the ether oxygen of the HPE polymer would increase the SLD of this layer. Previous work by Hamilton et al. indicates that Zn weakly interacts with the ether group of HPE polymer.[29] Thus, we ascribe the increased SLD of the first layer of NOHM-I-HPE with added $ZnCl_2$ salt to be due to the sequestration of Zn ions in this HPE layer. While the potential of increased D_2O loading in this layer cannot be discounted, the absence of this level of D_2O in the $KHCO_3$ solutions supports the presence of Zn ions as the dominant factor. Similarly, this increase in SLD is also observed in the NOHMs layer that assembles above the free polymer layer, further supporting the relevance of the interaction of Zn ions with HPE polymer that is grafted to the silica nanoparticles.

The fitting of the reflectivity curves shows that the near surface density profile of the NOHMs solutions change from 5 layers to 3 layers with the applied potential, the ordering of the structures near the surface changes from 5 layers to 3 layers before transitioning to bulk. Under the applied potential of -1.1 V, the first layer has an SLD of 3.39 with a thickness of ~16 Å. At 0V, the SLD of the first layer is lower than this layer, but the thickness remains similar. This indicates that the HPE polymer is not affected by the applied potential, however, more deuterated water molecule migrates in this layer. The loss of two layers in the SLD profile strongly suggests that the NOHMs nanoparticle no longer order at the surface in an applied potential. Rather, the SLD and thickness that emerge from the density profile suggest that the second layer is also dominated by a broad layer of HPE free polymer. The sequestration of free polymer towards the electrode surface could be due to the attractive interaction between free polymer and the negative potential at the electrode surface. The HPE polymers possess positively charged end groups that are meant to graft to the negatively charged SiO_2 nanoparticle surface. Thus, this

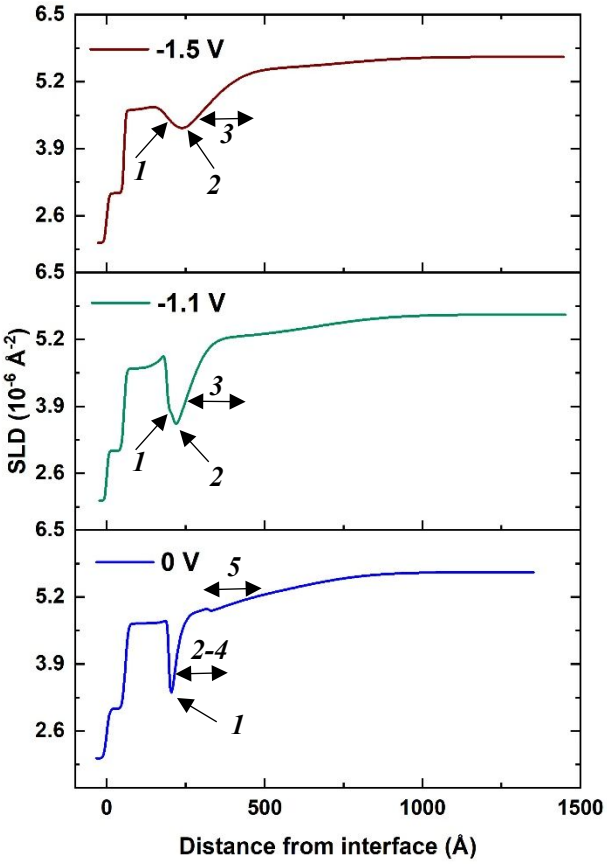

Figure 7 SLD profile of NOHM-I-HPE with $ZnCl_2$ salt in D_2O near Au surface at 0 V (bottom), -1.1 V (middle), -1.5 V (top). At 0 V, 5 layers are noted where *1* is the free polymer layer, *2-4* form the single NOHMs layer and *5* is the transition layer. At -1.1 V and -1.5 V, 3 layers are documented where *1,2* are the free polymer layers and *3* is the transition layer.

polymer will be attracted to the negatively charged electrode, driving its migration towards the electrode surface. Similar potential-dependent ordering is a common phenomenon in ionic liquid-based electrolytes where the ordering of cations and anions can be tuned by altering the potential.[38]

Table 4 SLD density profile that emerge the fit of the reflectivity of NOHM-I-HPE solution in the presence of $ZnCl_2$ salt at 0, -1.1, -1.5 V.

Sample	Potential	Parameters	Layer 1	Layer 2	Layer 3	Layer 4	Layer 5	Bulk
10 wt.% NOHM-I-HPE with $ZnCl_2$	**0 V**	SLD (10^{-6} Å^{-2}) ± error	2.88 ± 0.13	3.71 ± 0.27	4.95 ± 0.07	4.69 ± 0.04	5.06 ± 0.01	5.68
		Z (Å) ± error	15.5± 1.69	13.9 ± 0.82	98.62 ± 3.5	16.1 ± 2.44	234 ± 6.80	-
		R (Å) ± error	7.43 ± 1.25	9.73 ± 2.01	29.5 ± 5.10	5.32 ± 1.02	43.8 ± 34.0	182± 7.20
	-1.1 V	SLD (10^{-6} Å^{-2}) ± error	3.39 ± 0.15	2.40 ± 0.14	5.25 ± 0.05	-	-	5.68
		Z (Å) ± error	16.4 ± 2.62	38.3± 1.50	411± 15.57	-	-	-
		R (Å) ± error	8.30 ± 1.1	17.8 ± 3.68	54.2 ± 5.35	-	-	198± 7.0
	-1.5 V	SLD (10^{-6} Å^{-2}) ± error	3.94 ± 0.04	3.76 ± 0.02	5.50 ± 0.10	-	-	5.68
		Z (Å) ± error	39.5 ± 1.10	69.2 ± 4.78	466 ± 19.8	-	-	
		R (Å) ± error	24.8 ± 1.10	17.9 ± 2.20	98.8 ± 10.20	-	-	172± 7.20

Finally, the SLD and thickness of the upper (3rd) layer in the samples with applied potential is similar to the upper (5th) layer of the samples with no applied potential. Thus, we assign this layer to a transition layer from the ordered surface layers to the bulk.

The near surface ordering of the NOHMs changes dramatically when an applied potential is present. In the absence of an applied field, the reflectivity shows the presence of a fluctuating layer of NOHMs near the Au surface, however upon application of a potential, this near surface ordering is eliminated. This phenomenon is quite unique, however, not surprising considering that

the surface of the silica nanoparticles is functionalized with negatively charged linkers. Consequently, when a negative potential is applied to the electrode surface, we expect that there is a repulsion of the negatively charged NOHM surface and the electrode, disrupting the ordering of NOHMs near the surface. The loss of an ordered NOHMs layer frees that area to promote the assembly of additional free polymer near the surface. The freedom of movement of free polymer and the applied potential also facilitates the accumulation of Zn salt in close proximity to the surface.

Moreover, this data is also consistent with previous work by Hamilton et al. which shows that the deposition of Zn salt at the electrode surface starts at -1.3 V. In our reflectivity study, the SLD of the first layer further increases to 3.94 and its thickness by ~240% with the application of a potential of -1.5 V. The increase in SLD and roughness is consistent with the deposition of Zn salt on the Au surface. The SLD of the profile decreases with distance from the Au surface, which we ascribe to the assembly of the protonated HPE polymer immediately above the HPE/Zn layer on the electrode. With the increase in potential from -1.1 V to -1.5 V, the increased SLD of this layer suggests that the increased HPE loading also includes interacting Zn (II) ions in this layer. The upper most layer is again a transition layer between the ordered structure near the electrode surface and the bulk layer. The SLD of the transition layer is higher (5.50) at -1.5 V than the SLD of the transition layer (5.25) at -1.1 V, emphasizing the diffusion of protonated polymer from the transition layer to the first and second layer, which results in an increase the SLD of the transition layer.

Figure 8 provides an illustration of the density profile of the components in the NOHM-I-HPE solutions at 0 V and -1.5 V potential in the presence of $ZnCl_2$ salt. At 0 V, the free polymer assembles near the surface as the primary first layer, followed by a fluctuating NOHM-I-HPE layer

immediately above that. The coordination of Zn (II) with the free polymer and the grafted layer manifests as an increase in the SLD of the free and grafted polymer layers. Application of 1.5 V potential drives the Zn salt to sequester to the surface in the primary first layer. The ordering of the Zn at the surface is in agreement with the study by Hamilton et al. that observed the segregation of Zn to the electrode surface in similar NOHM-I-HPE samples. Above this near surface layer resides a free polymer-rich layer, which differs from the second layer of the NOHM-I-HPE sample at -1.1 V. This layer has a higher SLD and is thicker. The higher SLD indicates that this layer contains more D_2O, which also translates to a larger roughness, signifying a broader gradient to the transition layer. These analyses offer structural insight into the role of the HPE and/or NOHM-I-HPE on the deposition of Zn in these solutions as observed by Hamilton et al. In these studies, it was observed that the presence of HPE or NOHM-I-HPE in $ZnCl_2$ solutions drives a smooth deposition of Zn on the electrode surface and limits dendrite formation. The results presented here show that the ordering of free polymer and the interaction of free polymer with Zn provides an

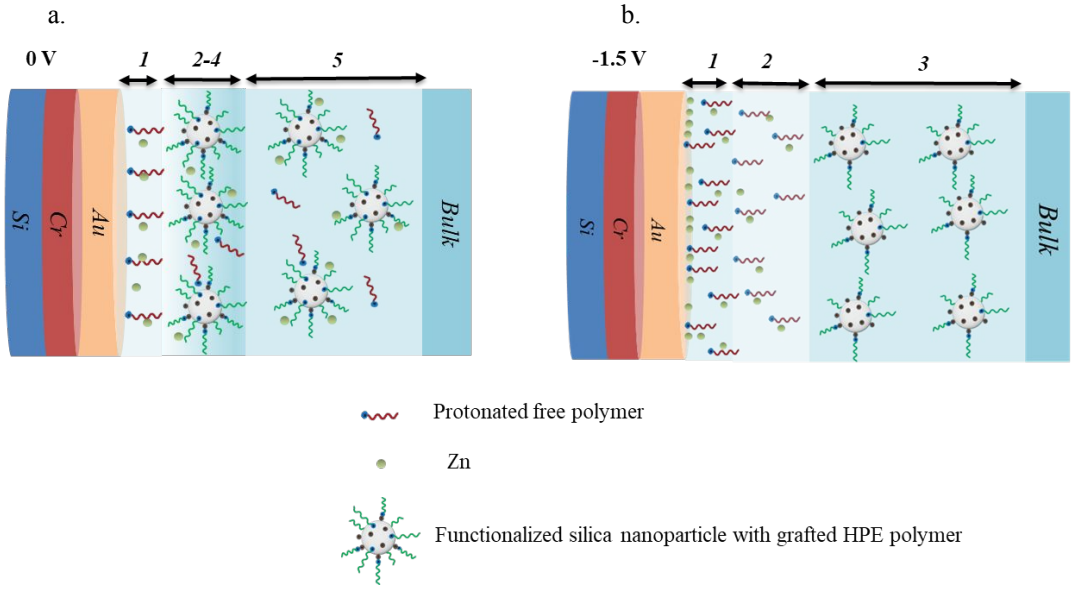

Figure 8 Ordering of free polymer and NOHM-I-HPE near the Au surface at 0 and -1.5 V. Figure 8a shows the ordering of free polymer (layer *1*) and NOHM-I-HPE near the surface that interacts with Zn (II) (layer *2-4*). Figure 8b shows the deposition of Zn (layer *1*), more ordering of free polymer (layer *2*) and disordering of NOHM-I-HPE near Au surface (layer *3*).

assembly of all components near the surface that benefits the smooth deposition of Zn on the electrode surface at the applied potential.

Impact of ordering of HPE and NOHM-I-HPE on Electrochemical performance

Neutron reflectivity results show that when free HPE polymer is in the aqueous solution in the presence of supporting electrolyte, at least two-three layers of unbound HPE polymer assembles near the Au and SiO_x surface (both surfaces will be considered as electrode surfaces for rest of the section). This assembly of HPE polymer can passivate the electrode surface and decrease available surface area for the electro-active species near the electrode surface, decreasing the probability of the redox reaction. Thus, this ordering of HPE polymer could eventually decrease the current density of an electrochemical system by decreasing the active sites near the electrode surface. In the case of the NOHM-I-HPE, a single layer of free polymer adsorbs near the electrode surface. Moreover, the supporting electrolyte may coordinate with the HPE polymer providing additional pathways for the ion to reach the electrode. This offers pathways for the supporting electrolyte to access the surface of the electrode, to increase current output relative to a solution with only to unbound HPE polymer. This interpretation is supported by the results presented by Hamilton et al. where $ZnCl_2$ solutions showed increased current density with the presence of NOHM-I-HPE additive relative to the sample with just HPE polymer.[29]

Conclusion

In this study, neutron reflectometry has been used to carefully monitor the ordering of the polymeric and naoparticle components, HPE and NOHM-I-HPE, of a promising electrolyte near electrode surfaces with varying surface chemistry and potential. The study indicates that a change in the hydrophilicity of the surface does not alter the ordering of the free polymer or NOHM-I-

HPE near the electrode surface. The addition of $KHCO_3$ salt in the HPE solution causes a kosmotropic effect, forcing layers of varying water composition to assemble near the surfaces. The results show that free polymer segregates to the electrode surface with a neighboring single layer of NOHM-I-HPE. Interestingly, the ordering of the NOHM-I-HPE layer does not significantly change with the addition of salt. Rather, the addition of salt, the collapses the grafted HPE polymer , as demnostrated in our previous work,[30] with little change in the depth profile of free polymer or NOHM-I-HPE. The application of a potential appear to disrupt the single layer of NOHM-I-HPE assembled near the Au surface. Additionally, more free polymer segregates to the surface with the applied potential. At the highest negative potential examined (-1.5 V), the near surface structure of the NOHM-I-HPE remains disordered with an increase in the amount of free polymer and Zn sequestered near the electrode surface. Correlating this assembly of free polymer and Zn on the electrode surface in a potential with a previous study by Hamilton et al., which shows a smooth deposition of Zn on the electrode surface in the presence of NOHM-I-HPE, suggests that the assembly of the free polymer near the electrode surface promotes the smooth deposition of Zn.[29] Therefore, the results presented in this study provide fundamental insight into the impact of the near surface assembly of free polymer and NOHM-I-HPE nanoparticles on the ultimate performance of NOHM-based electrochemical systems. [29] For instance, this work may have potential implications in CO_2 reduction (CO_2R) studies where structuring of water molecule near the electrode surface and the presence of cations with varying size may impact CO_2 reduction reactions.[51,52] Finally, to develop improved NOHMs based electrochemical systems, further experiments are needed to more fully elucidate the impact of the ordering of HPE polymer covalently bound to the nanoparticle surface (NOHM-C-HPE) near the electrode surface to their electrochemical performance.

Acknowledgement

This work was supported as part of the Breakthrough Electrolytes for Energy Storage (BEES), an Energy Frontier Research Center funded by the U.S. Department of Energy, Office of Science, Basic Energy Sciences under Award # DE-SC0019409. This research used resources used at the *Spallation Neutron Source, a DOE Office of Science User Facility operated by the Oak Ridge National Laboratory.*

Reference

(1) Yan, W.; Wang, C.; Tian, J.; Zhu, G.; Ma, L.; Wang, Y.; Chen, R.; Hu, Y.; Wang, L.; Chen, T.; Ma, J.; Jin, Z. All-Polymer Particulate Slurry Batteries. *Nat. Commun. 2019 101* **2019**, *10* (1), 1–11. https://doi.org/10.1038/s41467-019-10607-0.

(2) Janoschka, T.; Martin, N.; Martin, U.; Friebe, C.; Morgenstern, S.; Hiller, H.; Hager, M. D.; Schubert, U. S. An Aqueous, Polymer-Based Redox-Flow Battery Using Non-Corrosive, Safe, and Low-Cost Materials. https://doi.org/10.1038/nature15746.

(3) Luo, J.; Hu, B.; Hu, M.; Zhao, Y.; Liu, T. L. Status and Prospects of Organic Redox Flow Batteries toward Sustainable Energy Storage. *ACS Energy Lett.* **2019**, *4* (9), 2220–2240. https://doi.org/10.1021/ACSENERGYLETT.9B01332.

(4) Ding, Y.; Zhang, C.; Zhang, L.; Zhou, Y.; Yu, G. Molecular Engineering of Organic Electroactive Materials for Redox Flow Batteries. *Chem. Soc. Rev.* **2018**, *47* (1), 69–103. https://doi.org/10.1039/c7cs00569e.

(5) Li, Z.; Lu, Y. C. Material Design of Aqueous Redox Flow Batteries: Fundamental Challenges and Mitigation Strategies. *Adv. Mater.* **2020**, *32* (47), 2002132. https://doi.org/10.1002/ADMA.202002132.

(6) Liu, Y.; Chen, Q.; Sun, P.; Li, Y.; Yang, Z.; Xu, T. Organic Electrolytes for Aqueous Organic Flow Batteries. *Mater. Today Energy* **2021**, *20*, 100634. https://doi.org/10.1016/J.MTENER.2020.100634.

(7) Wang, W.; Xu, W.; Cosimbescu, L.; Choi, D.; Li, L.; Yang, Z. Anthraquinone with Tailored Structure for a Nonaqueous Metal–Organic Redox Flow Battery. *Chem. Commun.* **2012**, *48* (53), 6669–6671. https://doi.org/10.1039/C2CC32466K.

(8) Wang, X.; Chai, J.; Devi, N.; Lashgari, A.; Chaturvedi, A.; Jiang, J. "Jimmy." Two-Electron-Active Tetracyanoethylene for Nonaqueous Redox Flow Batteries. *J. Mater. Chem. A* **2021**, *9* (24), 13867–13873. https://doi.org/10.1039/D1TA01365C.

(9) Wang, Y.; Niu, Z.; Zheng, Q.; Zhang, C.; Ye, J.; Dai, G.; Zhao, Y.; Zhang, X. Zn-Based Eutectic Mixture as Anolyte for Hybrid Redox Flow Batteries OPEN. https://doi.org/10.1038/s41598-018-24059-x.

(10) Xu, Q.; Qin, L. Y.; Ji, Y. N.; Leung, P. K.; Su, H. N.; Qiao, F.; Yang, W. W.; Shah, A. A.; Li, H. M. A Deep Eutectic Solvent (DES) Electrolyte-Based Vanadium-Iron Redox Flow Battery Enabling Higher Specific Capacity and Improved Thermal Stability. *Electrochim. Acta* **2019**, *293*, 426–431. https://doi.org/10.1016/J.ELECTACTA.2018.10.063.

(11) Kawase, K.; Abe, J.; Tenjimbayashi, M.; Kobayashi, Y.; Takahashi, K.; Shiratori, S. Novel Deep-Eutectic-Solvent-Infused Carbon Nanofiber Networks as High Power Density Green Battery Cathodes. *ACS Appl. Mater. Interfaces* **2018**, *10* (18), 15742–15750. https://doi.org/10.1021/ACSAMI.8B03099.

(12) Imel, A. E.; Barth, B.; Hayes, D. G.; Dadmun, M.; Zawodzinski, T. Microemulsions as Emerging Electrolytes: The Correlation of Structure to Electrochemical Response. *ACS Appl. Mater. Interfaces* **2022**, *14* (17), 20179–20189. https://doi.org/10.1021/acsami.2c00181.

(13) Peng, J.; Cantillo, N. M.; Nelms, K. M. K.; Roberts, L. S.; Goenaga, G.; Imel, A.; Barth, B. A.; Dadmun, M.; Heroux, L.; Hayes, D. G.; Zawodzinski, T. Electron Transfer in Microemulsion-Based Electrolytes. *ACS Appl. Mater. Interfaces* **2020**, *12* (36), 40213–40219. https://doi.org/10.1021/ACSAMI.0C07028.

(14) Barth, B. A.; Imel, A.; Nelms, K. M. K.; Goenaga, G. A.; Zawodzinski, T. Microemulsions: Breakthrough Electrolytes for Redox Flow Batteries. *Front. Chem.* **2022**, *10*. https://doi.org/10.3389/FCHEM.2022.831200.

(15) Peng, J.; Xiao, Y.; Imel, A.; Barth, B. A.; Cantillo, N. M.; Nelms, K. M. K.; Zawodzinski, T. A. Electrolyte Effects on the Electrochemical Performance of Microemulsions. *Electrochim. Acta* **2021**, *393*, 139048. https://doi.org/10.1016/J.ELECTACTA.2021.139048.

(16) Feric, T. G.; Hamilton, S. T.; Cantillo, N. M.; Imel, A. E.; Zawodzinski, T. A.; Park, A. H. A. Dynamic Mixing Behaviors of Ionically Tethered Polymer Canopy of Nanoscale Hybrid Materials in Fluids of Varying Physical and Chemical Properties. *J. Phys. Chem. B* **2021**, *125* (32), 9223–9234. https://doi.org/10.1021/ACS.JPCB.1C00935.

(17) Hamilton, S. T.; Feric, T. G.; Bhattacharyya, S.; Cantillo, N. M.; Greenbaum, S. G.; Zawodzinski, T. A.; Park, A. A. Nanoscale Hybrid Electrolytes with Viscosity Controlled Using Ionic Stimulus for Electrochemical Energy Conversion and Storage. *JACS Au* **2022**. https://doi.org/10.1021/jacsau.1c00410.

(18) Cantillo, N.; Bruce, M.; Hamilton, S.; Feric, T.; Park, A.-H. A.; Zawodzinski, T. Electrochemical Behavior of Copper Ion Complexed with Nanoparticle Organic Hybrid Materials. *J. Electrochem. Soc.* **2020**, *167* (11), 116508. https://doi.org/10.1149/1945-7111/aba158.

(19) Feric, T. G.; Hamilton, S. T.; Haque, M. A.; Jeddi, J.; Sangoro, J.; Dadmun, M. D.; Park, A. H. A. Impacts of Bond Type and Grafting Density on the Thermal, Structural, and Transport Behaviors of Nanoparticle Organic Hybrid Materials-Based Electrolytes. *Adv. Funct. Mater.* **2022**, *32* (36). https://doi.org/10.1002/adfm.202203947.

(20) Petit, C.; Bhatnagar, S.; Park, A. H. A. Effect of Water on the Physical Properties and Carbon Dioxide Capture Capacities of Liquid-like Nanoparticle Organic Hybrid Materials and Their Corresponding Polymers. *J. Colloid Interface Sci.* **2013**, *407*, 102–108. https://doi.org/10.1016/J.JCIS.2013.05.065.

(21) Andrew Lin, K. Y.; Park, Y.; Petit, C.; Park, A. H. A. Thermal Stability, Swelling Behavior and CO2 Absorption Properties of Nanoscale Ionic Materials (NIMs). *RSC Adv.* **2014**, *4* (110), 65195–65204. https://doi.org/10.1039/c4ra10722e.

(22) Petit, C.; Lin, K.-Y. A. Y. A.; Park, A.-H. A. H. A. Design and Characterization of Liquidlike Poss-Based Hybrid Nanomaterials Synthesized via Ionic Bonding and Their Interactions with Co2. *Langmuir* **2013**, *29* (39), 12234–12242. https://doi.org/10.1021/la4007923.

(23) Moon, S.; Lee, Y.; Choi, S.; Hong, S.; Lee, S.; Park, A.-H. A.; Park, Y. Spectroscopic Investigation of Thermochemical Depolymerization of Lignin Model Compounds in the Presence of Novel Liquidlike Nanoparticle Organic Hybrid Solvents for Efficient Biomass Valorization. **2018**. https://doi.org/10.1021/acs.oprd.8b00282.

(24) Feric, T. G.; Hamilton, S. T.; Park, A. H. A. Insights into the Enhanced Oxidative Thermal Stability of Nanoparticle Organic Hybrid Materials Developed for Carbon Capture and Energy Storage. *Energy and Fuels* **2021**, *35* (23), 19592–19605. https://doi.org/10.1021/ACS.ENERGYFUELS.1C03243.

(25) Lin, K.-Y. A. Y. A.; Park, A. H. A. Effects of Bonding Types and Functional Groups on CO_2 Capture Using Novel Multiphase Systems of Liquid-like Nanoparticle Organic Hybrid Materials. *Environ. Sci. Technol.* **2011**, *45* (15), 6633–6639. https://doi.org/10.1021/es200146g.

(26) Rim, G.; Feric, T. G.; Moore, T.; Park, A. H. A. Solvent Impregnated Polymers Loaded with Liquid-Like Nanoparticle Organic Hybrid Materials for Enhanced Kinetics of Direct Air Capture and Point Source CO_2 Capture. *Adv. Funct. Mater.* **2021**, *31* (21), 2010047. https://doi.org/10.1002/ADFM.202010047.

(27) Overa, S.; Feric, T. G.; Alissa Park, A.-H.; Jiao, F. Tandem and Hybrid Processes for Carbon Dioxide Utilization. **2021**. https://doi.org/10.1016/j.joule.2020.12.004.

(28) Feric, T. G.; Hamilton, S. T.; Ko, B. H.; Lee, G. A.; Verma, S.; Jiao, F.; Park, A. H. A. Highly Tunable Syngas Product Ratios Enabled by Novel Nanoscale Hybrid Electrolytes Designed for Combined CO_2 Capture and Electrochemical Conversion. *Adv. Funct. Mater.* **2023**, 2210017. https://doi.org/10.1002/ADFM.202210017.

(29) Hamilton, S. T.; Feric, T. G.; Gładysiak, A.; Cantillo, N. M.; Zawodzinski, T. A.; Park, A. H. A. Mechanistic Study of Controlled Zinc Electrodeposition Behaviors Facilitated by Nanoscale Electrolyte Additives at the Electrode Interface. *ACS Appl. Mater. Interfaces* **2021**. https://doi.org/10.1021/acsami.1c23781.

(30) Haque, M. A.; Feric, T.; Hamilton, S.; Park, A.-H.; Dadmun, M. Structure and Dispersion of Free and Grafted Polymer in Nanoparticle Organic Hybrid Materials-Based Solutions by Small-Angle Neutron Scattering. *J. Phys. Chem. C 125* (9), 5327–5334. https://doi.org/10.1021/acs.jpcc.0c10790.

(31) Zhang, Y.; Chen, Z.; Qiu, H.; Yang, W.; Zhao, Z.; Zhao, J.; Cui, G. Pursuit of Reversible Zn Electrochemistry: A Time-Honored Challenge towards Low-Cost and Green Energy Storage. *NPG Asia Mater. 2020 121* **2020**, *12* (1), 1–24. https://doi.org/10.1038/s41427-019-0167-1.

(32) Zhao, Q.-Y.; Yin, G.-Y.; Liu, Y.-F.; Tang, R.-R.; Wu, X.-W.; Zeng, X.-X.; Xian-Xiang Zeng, C. Recent Advances in Material Chemistry for Zinc Enabled Redox Flow Batteries. *Carbon Neutralization* **2023**, *2* (1), 90–114. https://doi.org/10.1002/CNL2.43.

(33) Ma, L.; Pollard, T. P.; Zhang, Y.; Schroeder, M. A.; Ding, M. S.; Cresce, A. V.; Sun, R.; Baker, D. R.; Helms, B. A.; Maginn, E. J.; Wang, C.; Borodin, O.; Xu, K. Functionalized Phosphonium Cations Enable Zinc Metal Reversibility in Aqueous Electrolytes. *Angew. Chemie - Int. Ed.* **2021**, *60* (22), 12438–12445. https://doi.org/10.1002/anie.202017020.

(34) Zhang, D.; Warren, A. J.; Li, G.; Cheng, Z.; Han, X.; Zhao, Q.; Liu, X.; Deng, Y.; Archer, L. A. Electrodeposition of Zinc in Aqueous Electrolytes Containing High Molecular Weight Polymers. https://doi.org/10.1021/acs.macromol.0c00037.

(35) X-Ray and Neuron Reflectivity: Principles and Applications. *X-ray Neuron Reflectivity Princ. Appl.* **1999**. https://doi.org/10.1007/3-540-48696-8.

(36) Sears, V. F. Special Feature Neutron Scattering Lengths and Cross Sectioirn.

(37) Griffin, L. R.; Browning, K. L.; Clarke, S. M.; Smith, A. M.; Perkin, S.; Skoda, M. W. A.; Norman, S. E. Direct Measurements of Ionic Liquid Layering at a Single Mica–Liquid Interface and in Nano-Films between Two Mica–Liquid Interfaces. *Phys. Chem. Chem. Phys.* **2016**, *19* (1), 297–304. https://doi.org/10.1039/C6CP05757H.

(38) Nishi, N.; Uchiyashiki, J.; Ikeda, Y.; Katakura, S.; Oda, T.; Hino, M.; Yamada, N. L. Potential-Dependent Structure of the Ionic Layer at the Electrode Interface of an Ionic Liquid Probed Using Neutron Reflectometry. *J. Phys. Chem. C* **2019**, *123* (14), 9223–9230. https://doi.org/10.1021/acs.jpcc.9b01151.

(39) Lauw, Y.; Horne, M. D.; Rodopoulos, T.; Lockett, V.; Akgun, B.; Hamilton, W. A.; Nelson, A. R. J. Structure of [C 4 Mpyr][NTf 2] Room-Temperature Ionic Liquid at Charged Gold Interfaces. **2012**, *28*, 7381. https://doi.org/10.1021/la3005757.

(40) Klein, J. M.; Wang, H.; Sacci, R. L.; Browning, J. F.; Gurkan, B. Smooth Modified Surfaces of Silicon for the Study of Ionic Liquid Interfaces by Neutron Reflectometry. *ACS Appl. Electron. Mater.* **2021**. https://doi.org/10.1021/acsaelm.1c01351.

(41) Al-Shatty, W.; Campana, M.; Alexander, S.; Barron, A. R. Interaction of Surface-Modified Alumina Nanoparticles and Surfactants at an Oil/Water Interface: A Neutron Reflectometry, Scattering, and Enhanced Oil Recovery Study. *ACS Appl. Mater. Interfaces* **2022**, *14* (17), 19505–19514. https://doi.org/10.1021/ACSAMI.2C02228.

(42) Chung, E.; Yiacoumi, S.; Halbert, C.; Ankner, J.; Wang, W.; Kim, C.; Tsouris, C. Interaction of Silica Nanoparticles with a Flat Silica Surface through Neutron Reflectometry. *Environ. Sci. Technol.* **2012**, *46* (8), 4532–4538. https://doi.org/10.1021/es203992b.

(43) Vargas-Ruiz, S.; Soltwedel, O.; Micciulla, S.; Sreij, R.; Feoktystov, A.; Von Klitzing, R.; Hellweg, T.; Wellert, S. Sugar Surfactant Based Microemulsions at Solid Surfaces:

Influence of the Oil Type and Surface Polarity. *Langmuir* **2016**, *32* (45), 11928–11938. https://doi.org/10.1021/ACS.LANGMUIR.6B03441.

(44) Browning, K. L.; Sacci, R. L.; Doucet, M.; Browning, J. F.; Kim, J. R.; Veith, G. M. The Study of the Binder Poly(Acrylic Acid) and Its Role in Concomitant Solid-Electrolyte Interphase Formation on Si Anodes. *ACS Appl. Mater. Interfaces* **2020**, *12* (8), 10018–10030. https://doi.org/10.1021/acsami.9b22382.

(45) Nelson, A. Co-Refinement of Multiple-Contrast Neutron/X-Ray Reflectivity Data Using MOTOFIT. *J. Appl. Crystallogr.* **2006**, *39* (2), 273–276. https://doi.org/10.1107/S0021889806005073.

(46) Heroux, L. Structure Analysis of Soft Energy Materials Using Neutron Scattering. *Dr. Diss.* **2021**.

(47) Berton, P.; Kelley, S. P.; Bridges, N. J.; Klingshirn, M. A.; Huddleston, J. G.; Willauer, H. D.; Baldwin, J. W.; Moody, M. L.; Rogers, R. D. Water in Solutions of Chaotropic and Kosmotropic Salts: A Differential Scanning Calorimetry Investigation. *J. Chem. Eng. Data* **2019**, *64* (11), 4781–4792. https://doi.org/10.1021/acs.jced.9b00222.

(48) Collins, K. D.; Washabaugh, M. W. The Hofmeister Effect and the Behaviour of Water at Interfaces. *Q. Rev. Biophys.* **1985**, *18* (4), 323–422. https://doi.org/10.1017/S0033583500005369.

(49) Marcus, Y. Effect of Ions on the Structure of Water: Structure Making and Breaking. *Chem. Rev.* **2009**, *109* (3), 1346–1370. https://doi.org/10.1021/CR8003828/.

(50) Hughey, J. R.; Keen, J. M.; Miller, D. A.; Kolter, K.; Langley, N.; McGinity, J. W. The Use of Inorganic Salts to Improve the Dissolution Characteristics of Tablets Containing Soluplus®-Based Solid Dispersions. *Eur. J. Pharm. Sci.* **2013**, *48* (4–5), 758–766. https://doi.org/10.1016/J.EJPS.2013.01.004.

(51) Ringe, S.; Clark, E. L.; Resasco, J.; Walton, A.; Seger, B.; Bell, A. T.; Chan, K. Understanding Cation Effects in Electrochemical CO_2 Reduction. *Energy Environ. Sci.* **2019**, *12* (10), 3001–3014. https://doi.org/10.1039/c9ee01341e.

(52) Dunwell, M.; Yan, Y.; Xu, B. Understanding the Influence of the Electrochemical Double-Layer on Heterogeneous Electrochemical Reactions. *Current Opinion in Chemical Engineering*. Elsevier June 1, 2018, pp 151–158. https://doi.org/10.1016/j.coche.2018.05.003.